

# Non-resonant $n = 1$ helical deformation induced by $m/n = 2/1$ tearing mode in JT-60U

T. Bando<sup>1</sup>, S. Inoue<sup>1</sup>, A. Isayama<sup>1</sup>, K. Shinohara<sup>2</sup>, T. Wakatsuki<sup>1</sup>, M. Yoshida<sup>1</sup>, M. Honda<sup>1</sup>,  
G. Matsunaga<sup>1</sup>, M. Takechi<sup>1</sup>, N. Oyama<sup>1</sup>, and S. Ide<sup>1</sup>

<sup>1</sup>National Institutes for Quantum and Radiological Science and Technology, Naka, Ibaraki 311-0193, Japan

<sup>2</sup>The University of Tokyo, Kashiwa 277-8561, Japan

E-mail: bando.takahiro@qst.go.jp

## Abstract

In JT-60U, simultaneous excitation of  $n = 1$  helical cores (HCs) and  $m/n = 2/1$  Tearing Modes (TMs) was observed [T. Bando et al., *Plasma Phys. Control. Fusion* **61** 115014 (2019)]. In this paper, we report investigations of the excitation mechanism of  $n = 1$  HCs with  $m/n = 2/1$  TMs. In the previous study, it was reported that a “coupling” is observed between  $n = 1$  HCs and  $m/n = 2/1$  TMs: (1) The  $m/n = 2/1$  TM and the  $n = 1$  HC rotate keeping  $f_{m/n=1/1(\text{HC})} = 2f_{m/n=2/1(\text{TM})}$ . Here,  $f_{m/n=1/1(\text{HC})}$  and  $f_{m/n=2/1(\text{TM})}$  are the rotation frequency of the  $m/n = 1/1$  HC and the  $m/n = 2/1$  TM in the poloidal direction, respectively. (2) The core is shifted to the high-field side when the O-points of the  $m/n = 2/1$  magnetic island line up in the midplane. (3) The flux surfaces having the  $m/n = 2/1$  magnetic island have  $m/n = 1/1$  helical deformation (HD). The name of “helical deformation” means the deformation which is not localized at the core region. In this study, it is found that the coupling is observed with the mode frequency from several Hz to 6 kHz. This indicates that the resistive wall and the plasma control system do not induce the coupling. In addition, it is found that the coupling is observed even when  $q_{\min} > 1$ , indicating that  $n = 1$  HCs are the non-resonant mode. It is also confirmed that  $n = 1$  HCs does not rotate with the plasma in the core region, which indicates that  $n = 1$  HCs are not  $m/n = 1/1$  resonant modes localized at the core region. Accordingly, we propose a model of the excitation mechanism where the  $m/n = 1/1$  HD is induced directly by the current for the  $m/n = 2/1$  TM, which allows to excite the non-resonant  $m/n = 1/1$  mode. The model describes consistently characteristics of the coupling. Moreover, the model can explain the experimental observation; the fluctuation in the core region disappears with the stabilization of an  $m/n = 2/1$  neoclassical tearing mode by electron cyclotron current drive.

Keywords: Non-resonant mode, Helical core, Tearing mode, Magnetic island, Reduced MHD model, JT-60U, Tokamak

## 1. Introduction

Helical cores (HCs) in tokamaks have been an important research topic for the fusion reactor because HCs can affect transports of impurities [1-4], energetic particles [5], or toroidal momentum [5]. In addition to the effect on transport by helical structures, recent studies suggested that magnetohydrodynamics (MHD) dynamo accompanied with HCs redistributes the current profile in the core and realizes sawtooth-free plasmas of hybrid scenarios as observed in DIII-D [6,7], in which the minimum value of the safety factor profile,  $q_{\min}$ , is kept slightly above unity by “flux pumping”.

Several theoretical models to explain the excitation mechanism of HCs have been proposed. For example, the generation of the magnetic island by the excitation of tearing modes (TMs) due to the decrease of the electron temperature around the  $q = 1$  surface was proposed [8], which is induced by hydrogen pellet injection. This model intended to explain “snake” structure in soft X-ray (SX) emission, which was observed in JET [9]. HC equilibria can be obtained with  $q_{\min} \sim 1$  utilizing a three-dimensional MHD equilibrium solver [10,11], which is consistent with experimentally observed HCs in plasmas having  $q_{\min} \sim 1$  [4,12,13,14]. If the beta value is sufficiently high, the saturated  $m/n = 1/1$  quasi-interchange instability is excited and induce the dynamo loop voltage using 3D nonlinear simulations [15]. On the other hand, in recent experimental studies, HCs are induced by  $n = 1$  magnetic perturbation with the external coils and characteristics of HCs are investigated with taking account of reconstructed three-dimensional MHD equilibria in DIII-D [7,16,17]. The EAST team recently showed that the two-dimensional mode structure of a long-lived helical mode by combined use of tomography and a singular value decomposition, showing an  $m/n = 1/1$  mode structure and a substantial  $m/n = 2/2$  component where  $q_{\min}$  is kept slightly above unity [18].

Though many experimental and theoretical studies have been reported as mentioned above, the relationship between the mode structures of HCs and other MHD modes have not been discussed well. Recent our study [19] showed that a “coupling” is observed between  $n = 1$  HCs and  $m/n = 2/1$  TMs: (1) The  $m/n = 2/1$  TM and the  $m/n = 1/1$  HC rotate keeping  $f_{m/n=1/1(\text{HC})} = 2f_{m/n=2/1(\text{TM})}$ . Here,  $f_{m/n=1/1(\text{HC})}$  and  $f_{m/n=2/1(\text{TM})}$  are the rotation frequency of the  $m/n = 1/1$  HC and the  $m/n = 2/1$  TM in the poloidal direction, respectively. (2) The core is shifted to the high-field side when the O-points of the  $m/n = 2/1$  magnetic island line up in the midplane as shown in figure 1. (3) The flux surfaces having the  $m/n = 2/1$  magnetic island have  $m/n = 1/1$  “helical deformation”. In this study, the name of “helical deformation” indicates that the deformation which is not localized at the core region, and the “coupling” means coupling satisfying the three characteristics (1) ~ (3) mentioned in this paragraph. “ $m/n = 1/1$  helical deformation (HD)” means the  $m/n = 1/1$  deformation of the whole torus plasma, including the concept of the  $m/n = 1/1$  HC.

In the previous study, however, though possible excitation mechanisms of HCs were proposed such as the effect of the resistive wall where the resistive wall time  $\tau_w \sim 10$  ms [20] in JT-60U or helical equilibria with  $q_{\min} \sim 1$ , these candidates were not investigated. This is because the coupling was only studied with TMs having low mode frequencies ( $\leq 20$  Hz), mentioned as Low Frequency Mode (LFM) in the previous study [19], and the  $q$ -profile was not calculated mainly due to the long time scale of the mode frequency of LFM compared to the smoothing width of signals to calculate the MHD equilibrium. It is also required to investigate whether the plasma control system, where the time interval of the control of the plasma position is 250  $\mu$ s (4kHz), can induce HCs or not.

In this paper, we report investigations of the excitation mechanism of  $n = 1$  HCs based on the previous study [19]. It is found that the mode frequency with the coupling is 6 kHz, which indicates that the resistive wall and the plasma control system do not induce the coupling. In addition, it is found that the coupling is observed even when  $q_{\min} > 1$ , indicating that  $m/n = 1$  HCs are a non-resonant mode. In addition, it is confirmed that  $m/n = 1/1$  HCs do not rotate with the plasma in the core region by means of the comparison of the plasma rotation frequency and the mode frequency. Finally, we propose a model of the excitation mechanism where the  $m/n = 1/1$  HD is induced directly by the current for the  $m/n = 2/1$  magnetic island. The model consistently describes the observed characteristics of the coupling between  $m/n = 1/1$  HCs and  $m/n = 2/1$  TMs.

This article is organized as follows: In section 2, the heating system and diagnostic of JT-60U are introduced. In section 3, the investigations of  $m/n = 1/1$  HCs with  $m/n = 2/1$  neoclassical tearing modes (NTMs) with the mode frequencies of several kHz are introduced in subsection 3.1 first, then, the observation of an  $m/n = 1/1$  HC, where  $q_{\min}$  would be greater than unity, is introduced in subsection 3.2. In these subsections, the observed mode structures are compared with the characteristics (1) ~ (3) of the coupling mentioned in this section. The model we propose is described in section 4. In section 5, discussion mainly regarding the proposed model is given. The study is summarized in section 6.

## 2. Heating system and diagnostic of JT-60U

JT-60U is a tokamak device where typical major radius is 3.4 m and typical minor radius is 0.9 m [21]. The toroidal direction of the toroidal magnetic field and the plasma current is the clockwise direction in the analyzed discharges. In JT-60U, plasmas are heated by eleven neutral beam injectors (NBIs) with positive-ion source (P-NBI), whose acceleration energies are about 85 keV. Two (#9 and #10) of the tangential P-NBIs are co-current direction (co-direction) and other two (#7 and #8) tangential P-NBIs are counter-current direction (ctr-direction). Here, the co-direction and the ctr-direction are defined as the same direction and the opposite direction to the plasma current, respectively. The other seven NBs inject neutral beams to the plasma perpendicularly (PERP P-NBI). The electron cyclotron heating (ECH) with gyrotron is also available. The ECH is used to stabilize NTMs by electron cyclotron current drive (ECCD) [22] as well as to heat plasmas.

Figure 2 shows the sight lines of SX measurement (Upper SX) and the measured plane by electron cyclotron emission (ECE) measurement by heterodyne radiometers [23] and the polychromator [24], which are used to study the radial mode structure. The MHD equilibrium in figure 2 is obtained at 9.5 s of 49713 (figures 3, 5, and 6). The difference in the toroidal angle of the locations of SX measurement and ECE measurement are about 160 degrees. The ion temperature and the toroidal velocity are measured by charge exchange recombination spectroscopy (CXRS) [25], which is the same as CXRS1 in [19]. The toroidal and poloidal mode numbers are estimated with magnetic probes arranged toroidally and poloidally. The profile of the safety factor ( $q$ ) is calculated with 16 channels of the motional Stark effect (MSE) measurement [26,27] on the P17 port of JT-60U, which measures the polarization angles from the core region to the edge region of plasmas. The  $q$ -profile is reconstructed with the MEUDAS code [28] to reconstruct MHD equilibria assuming the toroidally axisymmetric geometry by solving the Grad-Shafranov equation. The MHD equilibrium is reconstructed so that the  $q$ -profile from the MHD equilibrium is consistent with the  $q$ -profile from the polarization angle of MSE measurement in the P17 port. The reconstructed MHD equilibrium can be obtained every 0.01 s, which is determined by the time resolution of the polarization angle from MSE measurement.

### 3. Experimental condition of observation of $m/n = 1$ HC with $m/n = 2/1$ TM

#### 3.1 $m/n = 1$ HC with $m/n = 2/1$ NTM whose frequency is several kHz

$n = 1$  HCs with  $m/n = 2/1$  NTMs are investigated with plasmas where NTMs occur and are stabilized by ECCD [22]. The plasma parameters in the analyzed plasmas are shown in table 1. In these discharges, NTMs are excited by the high injection power ( $\sim 20$  MW) of NBI and then the mode frequency of NTMs are increased with the increased toroidal rotation velocity by the tangential NBIs. As results, the mode frequencies of NTMs become several kHz. Due to the large net toroidal torque to the ctr-direction, the rotation directions of NTMs are the ctr-direction toroidally in discharges of table 1 when the mode frequencies of  $m/n = 2/1$  NTMs are several kHz.

Figure 3 shows typical time evolution of signals in the analyzed discharges. In this discharge, the total injection power of NBIs is about 20 MW from 4.9 s. With the high injection power, an NTM is excited around 5.92 s and the mode frequency decreases to almost zero Hz, which seems to be due to the toroidal torque by to the eddy current on the vacuum vessel [30]. The large  $b_r$  around 6 s in figure 3 (b) indicates the amplitude ( $\sim 2.5 \cdot 10^{-4}$  T) of the mode rotating slowly like LFMs reported in the previous study [19]. As the toroidal torque to ctr-direction increases and  $\beta_p$  (an indicator of the saturated size of the magnetic island of NTMs [31]) decreases, the mode frequency increases to several kHz as indicated by the red peak of coherence from 7.5s to 10.8s in figure 3 (c). The  $m/n = 2/1$  structure is observed with magnetic probes and the phase inversion around the  $q = 2$  surface with ECE measurement in figure 5 (b) are also observed indicating that the observed mode is an  $m/n = 2/1$  NTM.

In the analyzed discharges shown in table 1, the  $m = 1$  structure is observed with  $m/n = 2/1$  NTMs. In figure 4, the coherent fluctuations are observed in magnetic signals, SX signals, and the electron temperature with the mode frequency of the  $m/n = 2/1$  NTM. As seen in figure 4 (b) and (c), the phase of the fluctuation component of the SX signals and the electron temperature are inverted across  $\rho = 0$  in SX and ECE measurement, which indicates the existence of rotating  $m = 1$  structure. Here,  $\rho$  is the volume-averaged minor radius. This  $m = 1$  structure seems to have  $n = 1$  structure because the relationship between the phase profiles around  $\rho = 0$  in SX measurement and ECE measurement (figure 4 (b) and (c)) can be reproduced in synthetic images assuming the existence of the  $m/n = 1/1$  mode structure in the core, which is the same method as a method in the previous study [19]. The same observed mode frequency of the  $n = 1$  HC and the  $m/n = 2/1$  NTM may be corresponding to the characteristic (1) of the coupling mentioned in section 1. If the rotation frequency of the  $m/n = 1/1$  structure in the poloidal direction is twice as large as that of the  $m/n = 2/1$  structure, the observed mode frequencies become the same. This is explained with equations in section 4. Note that, in this study, the  $m = 1$  structure is not measured with magnetic probes arranged poloidally. This might be due to the small amplitude of the  $m = 1$  component compared with the  $m = 2$  component.

Because the observed mode frequencies of the  $m/n = 2/1$  NTM and the  $n = 1$  HC are the same, the phase profile can be evaluated from the core to the edge on these modes as shown in figure 5. As shown in figure 5 (a) and (b), the phase profile of  $m = 1$  structure in SX signals and the  $m/n = 2/1$  NTM around the  $q = 2$  surface (the phase difference  $\pi$  around the  $q = 2$  surface of figure 5 (d)) in ECE signals are not changed at 9 s, 9.3 s, and 9.5 s. The unchanged profiles indicate that the phases are locked (phase locking). Note that, in figure 5 (b), the change of the phase is just  $0.14\pi$  rad. across  $\rho = 0$  and is significant in the high field side where the sign of  $\rho$  is minus. This is because the difference of the poloidal angles of the measured points across  $\rho = 0$  is not  $\pi$  rad. on the horizontal plane for ECE measurement as seen in figure (2). In figure 5 (c), the estimated phases projected on the midplane are shown assuming the measured points of ECE measurement are moved to the midplane keeping the measured minor radius. As seen in the estimated phase profile of figure 5 (c), the difference of the phase across  $\rho = 0$  is about  $\pi$  rad., indicating  $m = 1$  structure. This method to modify the phase is valid when the single mode having a certain poloidal number covers the region for the estimation. In this case, the existence of  $m = 1$  mode structure in the core region is confirmed by SX measurement in figure 5 (a). The detailed description of the modification is found in Appendix A.

In relation to the phase locking in figure 5 (b), it is confirmed that the observed phase profile of ECE measurement can be reproduced in synthetic images assuming the coupling, indicating that the observed phase locking is consistent with the characteristics (1) and (2) of the coupling. In addition, the same phase from  $\rho = 0.1$  to  $\rho = 0.5$  is considered due to the  $n = 1$  HD from the core to the edge region (characteristic (3) of the coupling). Therefore, observed  $n = 1$  HCs with  $m/n = 2/1$  NTMs, whose mode frequencies are several kHz, seem to have characteristics (1) ~ (3) of the coupling. Because the observed mode frequency with the coupling can be several kHz in this study as well as  $\sim 20$  Hz in the previous study [19], the resistive wall does not induce the coupling. In addition, the coupling is observed when the mode frequency of an  $m/n = 2/1$  NTM is 6 kHz. This indicates that the observed HCs (HDs) are not induced by the plasma control system of JT-60U, which controls the position of the plasma with 4 kHz by changing the coil current.

As indicated in figure 4, the  $n = 1$  HC and the  $m/n = 2/1$  NTM have the same mode frequency. If the observed  $n = 1$  HC rotates with the background plasma like NTMs, the relationship,  $f_{\text{mode}} \sim n \times f_{\text{tor}} - m \times f_{\text{pol}}$ , should be satisfied [32]. Here,  $f_{\text{mode}}$  is the “observed” mode frequency,  $f_{\text{tor}}$  is the toroidal rotation frequency defined by  $V_{\text{tor}}/(2\pi R_m)$ , and  $f_{\text{pol}}$  is the poloidal

rotation frequency defined by  $V_{\text{pol}}/(2\pi\rho_m)$ . Here,  $V_{\text{tor}}$  ( $V_{\text{pol}}$ ),  $R_m$ , and  $\rho_m$  are the toroidal (poloidal) rotation velocity, the major radius where  $V_{\text{tor}}$  is measured, and the minor radius where  $V_{\text{pol}}$  is measured, respectively. In this study,  $f_{\text{pol}}$  is ignored because the net toroidal torque induced by the tangential NBIs are applied and  $V_{\text{tor}}$  is sufficiently larger than  $V_{\text{pol}}$  estimated with the CHARROT code [33,34] assuming the effective ion charge  $Z_{\text{eff}}$  is 2. The absolute values of the poloidal flow of the background deuteron plasma are smaller than 0.6 km/s from core region to the edge region. Figure 6 shows the radial profile of (a)  $V_{\text{tor}}$  measured by CXRS measurement and (b)  $f_{\text{tor}}$  at 9.5 s of 49713 in figure 3, assuming that the rotation velocity of the background deuteron plasma and the carbon plasma as impurity are the same. The purple dashed line in figure 6 (a) is the calculated toroidal rotation velocity profile of the deuteron by the CHARROT code. The profile of the toroidal rotation velocity by CXRS measurement and the profile by the CHARROT code are consistent, indicating that it is valid to use  $V_{\text{tor}}$  of carbon plasma as the rotation velocity of the background deuteron plasma. The mode frequency of the  $m/n = 2/1$  NTM in figure 3 (c) is about 2.3 kHz and is consistent with  $f_{\text{tor}}$  around the  $q = 2$  surface as seen in figure 6 (b). On the other hand, in the case of the  $m/n = 1/1$  HC, the corresponding  $f_{\text{tor}}$  is not observed in the core region. This indicates that the observed  $m/n = 1/1$  HC cannot be explained by the rotation at the  $q = 1$  surface which seems to be located at the core region in the plasma. In the other words, there is a possibility that the observed  $n = 1$  HC is a non-resonant mode.

### 3.2. $m/n = 1$ HC with $m/n = 2/1$ TM with $q_{\text{min}} > 1$

As mentioned in subsection 3.1, the existence of the  $q = 1$  surface is important information to distinguish the  $m/n = 1/1$  non-resonant mode from the  $m/n = 1/1$  resonant mode. However, in figure 5 (d), the  $q$ -profile is the normal shear where  $q_{\text{min}}$  can be smaller than unity. It is better to examine whether the  $m/n = 1/1$  structure is observed with  $q_{\text{min}} \gg 1$  or not. This is examined at 7.55 s in 48885 shown in figure 7 where an  $m/n = 2/1$  TM is observed. The plasma discharge 48887 is for a high  $\beta$  plasma experiment [35] and it is tried to make weak shear profile for forming the internal transport barrier (ITB). With the weak shear profile,  $q_{\text{min}}$  tends to greater than unity. In this discharge, the mode frequency of the  $m/n = 2/1$  TM is relatively slow ( $\sim$  Hz) after the decrease of the mode frequency at 7.55 s. This low frequency mode is the same object as the LFM described in the previous study [19].

The extended view is shown in figure 8 (a) and (b). At 7.55 s, the plasma parameters are the plasma current  $\sim 0.9$  MA, the magnitude of magnetic field at magnetic axis  $\sim 1.52$  T, the major radius  $\sim 3.43$  m, the minor radius  $\sim 0.92$  m, the radial position of axis is 3.53 m, the vertical position of axis is 0.2 m, the plasma elongation  $\sim 1.39$ , the plasma triangularity  $\sim 0.38$ , the plasma volume  $\sim 72$  m<sup>3</sup>, and  $q_{95} \sim 3.5$ . This discharge is made after the installation of ferrite steel tiles on the vacuum vessel to reduce the toroidal magnetic field ripple [29]. In figure 8 (a), the  $n = 1$  mode, whose mode frequency is about 200 Hz, is observed in the magnetic fluctuation before 7.55 s. And in figure 8 (b), the fluctuation of the electron temperature from ECE measurement showing fluctuation of the  $n = 1$  mode is observed. In figure 8 (b), because the  $q = 2$  surface locates around  $\rho = 0.6$  and the phases of the fluctuations are inverted between  $\rho \sim 0.50$  and  $\rho \sim 0.57$ , the observed  $n = 1$  mode seems to be an  $m/n = 2/1$  TM. The rotation direction of the  $m/n = 2/1$  TM is the ctr-direction toroidally. As well as the phases around  $q = 2$  surface, the phases are inverted between signals from  $\rho \sim -0.13$  and  $\rho \sim 0.24$  in figure 8 (b), indicating the  $m = 1$  structure. Here, the difference in the poloidal angle between the measured points across  $\rho \sim 0$  are about  $\pi$  rad. unlike the case in figure 5 (b) because the vertical position of axis and the measured plane by ECE measurement are on the same horizontal plane. This  $m = 1$  structure is also observed with SX measurement. Because the relationship between the phase profile around  $\rho = 0$  in ECE and SX measurement around 7.55 s can be reproduced in synthetic images assuming the existence of the  $m/n = 1/1$  mode structure in the core, the observed  $m = 1$  structure seems to have  $n = 1$  structure, which is the same as the result in the previous subsection.

As seen in figure (8), the differences of the phases from core to the  $q = 2$  surface are not changed in time, indicating the phase locking. In addition, it is confirmed that the observed phase profile of ECE measurement can be reproduced in synthetic images assuming the coupling, indicating that the observed phase locking is consistent with the characteristics (1) and (2) of the coupling. The same phase from the core to the  $q = 2$  surface is observed and this observation is consistent with characteristic (3) of the coupling. Therefore, the observed  $n = 1$  HC with the  $m/n = 2/1$  TM in this subsection seems to have characteristics (1)  $\sim$  (3) of the coupling.

The  $q$ -profile estimated with the MEUDAS code is shown in figure 8 (c). In this estimation, the polarization angle is averaged from 7.54 s to 7.56 s for the reconstruction of the MHD equilibria to average the non-axisymmetric effect of the mode structure. As shown in figure 8 (c),  $q_{\text{min}}$  at 7.55 s is about 1.4  $> 1$ , namely  $q_{\text{min}} > 1$ , indicating that the observed  $m/n = 1/1$  mode is a non-resonant mode.

#### 4. Model where $m/n = 1/1$ HD directly induced by $m/n = 2/1$ TM

As reported in the previous section, the non-resonant  $n = 1$  HC coupled with the  $m/n = 2/1$  TM is observed. However, it is difficult to explain the excitation of the  $n = 1$  HC and characteristics of the coupling by the theory proposed in the previous studies [8,10,11,15]. Through the investigations in section 3, it is found that the resistive wall and the plasma control system do not induce the coupling. Therefore, it is likely to consider that the  $m/n = 1/1$  HD is induced by the  $m/n = 2/1$  TM. Here, we propose a model where the  $m/n = 2/1$  current for the magnetic island directly induces the  $m/n = 1/1$  HD. This model includes the non-resonant characteristics and is consistent with the observed characteristics of the coupling as discussed later.

In this model, we treat the reduced MHD model in a straight field-line coordinate system  $(r, \theta, \varphi)$  with the torus plasma having the circular poloidal cross section. With the straight field-line coordinate system, because  $\nabla \cdot \mathbf{B} = 0$ ,

$$\mathbf{B} = \nabla\varphi \times \nabla\psi + \nabla\theta \times \nabla\chi \quad (1)$$

is obtained. Here,  $\psi$  and  $\chi$  are the poloidal flux and the toroidal flux, respectively. Because the component with  $\chi$  is ignored with the reduced MHD model, the magnetic field can be expressed as  $\mathbf{B} = \nabla\varphi \times \nabla\psi$ . The plasma current  $\mathbf{J}$  is obtained with  $\mathbf{J} = \nabla \times \mathbf{B}$ . Here, we expand the quantities by means of Fourier transform for  $(\theta, \varphi)$  directions. An arbitrary quantity  $X$  is expanded as  $X = \sum_{m,n=-\infty}^{\infty} \tilde{X}_{m,n}$ ,  $\tilde{X}_{m,n} = X_{m,n} e^{i(m\theta+n\varphi)}$ . The derivatives are expressed as  $\frac{\partial \tilde{X}_{m,n}}{\partial \theta} = im\tilde{X}_{m,n}$  and  $\frac{\partial \tilde{X}_{m,n}}{\partial \varphi} = in\tilde{X}_{m,n}$ .

If there is a magnetic island at  $q = m/n$  rational surface, the  $m/n$  component  $j_{m,n}^{\varphi}$  is dominant. The  $j_{m,n}^{\varphi}$  component is written as

$$j_{m,n}^{\varphi} = \sum_{m'+m''=m} g_{m'}^{rr} \frac{\partial^2 \psi_{m',n}}{\partial r^2} + \left[ \frac{1}{r} \frac{\partial}{\partial r} (r g_{m''}^{rr}) - (m+m') g_{m''}^{r\theta} \right] \frac{\partial \psi_{m',n}}{\partial r} - m' \left[ \frac{1}{r} \frac{\partial}{\partial r} (r g_{m''}^{r\theta}) + m g_{m''}^{\theta\theta} \right] \psi_{m',n} \quad (2).$$

The  $m'$  and  $m''$  are selected so that  $m' + m'' = m$ .  $g_m^{rr}$ ,  $g_m^{\theta\theta}$ , and  $g_m^{r\theta}$  are the  $m$ -th component of the Fourier expansion in the poloidal direction of  $g^{rr}$ ,  $g^{\theta\theta}$ , and  $g^{r\theta}$ , which are the component of the metric tensor. The toroidal variation of the metric tensor is ignored with the axisymmetric toroidal configuration. If  $m' = m$  and  $m'' = \pm 1$ , the sideband current of  $j_{m,n}^{\varphi}$  through  $\psi_{m,n}$  is estimated as

$$j_{m\pm 1,n}^{\varphi} \sim g_{\pm 1}^{rr} \frac{\partial^2 \psi_{m,n}}{\partial r^2} + \left[ \frac{1}{r} \frac{\partial}{\partial r} (r g_{\pm 1}^{rr}) \mp 2m g_{\pm 1}^{r\theta} \right] \frac{\partial \psi_{m,n}}{\partial r} - m \left[ \frac{1}{r} \frac{\partial}{\partial r} (r g_{\pm 1}^{r\theta}) + m g_{\pm 1}^{\theta\theta} \right] \psi_{m,n} \quad (3).$$

The  $m = \pm 1$  component of the metric tensor ( $g^{rr}$ ,  $g^{\theta\theta}$ , and  $g^{r\theta}$ ) with the circular poloidal cross section is found to be

$$g_{\pm 1}^{rr} = 2\epsilon r \quad (4)$$

$$g_{\pm 1}^{\theta\theta} = (2\epsilon)/r \quad (5)$$

$$g_{\pm 1}^{r\theta} = 0 \quad (6)$$

, which indicate that the  $m = \pm 1$  component of  $g^{rr}$  and  $g^{\theta\theta}$  exist with the order of the inversion of the aspect ratio  $\epsilon$ . The  $m = \pm 1$  components with Shafranov shift and the non-circular effect are ignored. The  $m = \pm 1$  components with the order of  $\epsilon^2$  are also ignored. With equations (3) ~ (6), the sideband current  $j_{m\pm 1,n}^{\varphi}$  is expressed as

$$j_{m\pm 1,n}^{\varphi} \sim g_{\pm 1}^{rr} \frac{\partial^2 \psi_{m,n}}{\partial r^2} + \frac{1}{r} \frac{\partial}{\partial r} (r g_{\pm 1}^{rr}) \frac{\partial \psi_{m,n}}{\partial r} - m^2 g_{\pm 1}^{\theta\theta} \psi_{m,n} \quad (7).$$

The vector potential  $\mathbf{A}$  is written as

$$\mathbf{A} = -\psi \nabla\varphi \quad (8).$$

The relationship between the electric field  $\mathbf{E}$  and the vector potential  $\mathbf{A}$  is written as

$$\mathbf{E} = -\frac{\partial \mathbf{A}}{\partial t} - \nabla\alpha \quad (9).$$

$\alpha$  is the electrostatic potential and ignored in this model. The Ohm's law is expressed as

$$\mathbf{E} = \eta \mathbf{J} - \mathbf{V} \times \mathbf{B} \quad (10).$$

$\eta$  is the resistivity.  $\mathbf{V}$  is the plasma flow and the  $\mathbf{V} \times \mathbf{B}$  term is neglected in this model. With equations (7), (8), (9), and (10),

$$\frac{\partial}{\partial t} \psi_{m\pm 1, n} \sim \eta j_{m\pm 1, n}^{\varphi} \quad (11)$$

is obtained for the linear phase. Equation (11) means that  $\psi_{m\pm 1, n}$  component is induced by  $j_{m\pm 1, n}^{\varphi}$  with the  $m/n$  magnetic island. Note that the rational surface  $q = (m \pm 1)/n$  is not necessary to induce  $j_{m\pm 1, n}^{\varphi}$  current. This means that non-resonant structure can be induced.

If the  $m/n = 2/1$  mode and the  $m/n = 1/1$  mode occur, the phases of  $\tilde{\psi}_{2,1}$  and  $\tilde{\psi}_{1,1}$  with the rotating plasma can be written as [36]

$$\arg(\tilde{\psi}_{2,1}) = \varphi + 2\theta + (\omega_{2,1})_{\text{mode}} t + \delta_{0(2,1)} \quad (12)$$

$$\arg(\tilde{\psi}_{1,1}) = \varphi + \theta + (\omega_{1,1})_{\text{mode}} t + \delta_{0(1,1)} \quad (13).$$

$(\omega_{2,1})_{\text{mode}}$  and  $(\omega_{1,1})_{\text{mode}}$  are the observed mode frequency of the  $m/n = 2/1$  mode and the  $m/n = 1/1$  mode in the laboratory system, respectively.  $\delta_{0(2,1)}$  and  $\delta_{0(1,1)}$  are the initial phase of  $\tilde{\psi}_{2,1}$  and  $\tilde{\psi}_{1,1}$ , respectively. The observed poloidal rotation frequency of  $\tilde{\psi}_{m,n}$  is expressed as  $(\omega_{m,n})_{\text{pol}}$ .  $(\omega_{m,n})_{\text{mode}} = m(\omega_{m,n})_{\text{pol}}$  is satisfied. If the  $m/n$  mode directly induces the  $(m-1)/n$  mode, the rotating  $m/n$  mode is accompanied by the  $(m-1)/n$  mode should satisfy the relationship  $\frac{2\pi}{m-1} : \frac{2\pi}{m} = (\omega_{m-1,n})_{\text{pol}} : (\omega_{m,n})_{\text{pol}}$ . Therefore,  $(\omega_{1,1})_{\text{pol}} = 2(\omega_{2,1})_{\text{pol}}$  is obtained, which is consistent with the characteristic (1) of the coupling,  $f_{m/n=1/1(\text{HC})} = 2f_{m/n=2/1(\text{TM})}$ .  $(\omega_{1,1})_{\text{pol}} = 2(\omega_{2,1})_{\text{pol}}$  indicates  $(\omega_{1,1})_{\text{mode}} = (\omega_{2,1})_{\text{mode}}$ , which is consistent with the same observed mode frequency in subsection 3.1.

In this study, the characteristic (2) of the coupling is partially explained. When the phase difference between the two modes is defined as  $\Delta \equiv \arg(\tilde{\psi}_{2,1}) - \arg(\tilde{\psi}_{1,1}) = \theta + \delta_{0(2,1)} - \delta_{0(1,1)}$ , the variation of  $\Delta$  is  $\pi$  rad. if the variation of  $\theta$  is  $\pi$  rad.. This is consistent with the characteristic (2) of the coupling as seen in figure 1. However, we have not found the equation of  $\delta_{0(2,1)} - \delta_{0(1,1)}$  so that  $\delta_{0(2,1)} - \delta_{0(1,1)} = \text{zero rad.}$  in the high field side in the midplane and  $\delta_{0(2,1)} - \delta_{0(1,1)} = \pi$  rad. in the low field side in the midplane, which is consistent with the view in figure 1. Here,  $\theta$  is defined as zero rad. in the low field side of the midplane. The theoretical explanation of the phase locking with the dynamical stability in [36] and its experimental validation in [37] would be helpful to induce the equation to explain the characteristic (2) with the proposed model.

It is worth to mention that the observed HD (characteristic (3) of the coupling) is consistent with the proposed model because the  $m/n = 1/1$  sideband current from the  $m/n = 2/1$  current can deform the whole plasma which is not localized at a certain flux surface. In addition, the observation that  $f_{\text{tor}}$  corresponding to  $m/n = 1/1$  HC is not observed in the core region mentioned in subsection 3.1 is also explained by the proposed model because the mode frequency is determined by the mode frequency of the  $m/n = 2/1$  TM.

According to the proposed model, the  $n = 1$  HC should disappear when the  $m/n = 2/1$  NTM is stabilized. This is examined in 49573 which is one of the series of discharges in table 1. In figure 9 (a), the signals from  $\rho \sim 0.1$  (red) and from  $\rho \sim 0.6$  (blue) show the  $m/n = 2/1$  component (fluctuations due to the  $m/n = 2/1$  NTM) of the electron temperature from ECE measurement by means of the band pass filter by Fourier Transform. Figure 9 (b) shows the  $m/n = 2/1$  component of the amplitude of magnetic fluctuations. The black line indicates the pattern of ECH (ECCD) around  $q = 2$  surface to stabilize the  $m/n = 2/1$  NTM. With the ECCD, according to the magnetic fluctuation in figure 9 (b), the  $m/n = 2/1$  NTM is stabilized around 11 s as indicated by the vertical dashed red line. The fluctuation from core and  $q = 2$  surface in figure 9 (a) also disappear until the vertical red line. As well as this discharge, the fluctuation of ECE signals from the core is observed until the  $m/n = 2/1$  magnetic fluctuation and the  $m/n = 2/1$  fluctuation of ECE signals from the  $q = 2$  surface disappear in the analyzed discharges of table 1. These observations are consistent with the proposed model where the  $m/n = 2/1$  TM directly induce the  $m/n = 1/1$  HD.

## 5. Discussion

In this study, experimental observations which suggest non-resonant  $m/n = 1/1$  HCs coupled with  $m/n = 2/1$  TMs are introduced and the model to be consistent with the observations is proposed. In the proposed model, the  $m/n = 1/1$  HD is induced directly by the current for the  $m/n = 2/1$  TMs.

The main difference in the excitation mechanism between the proposed model and other models [8,10,11,15] is the requirement of the corresponding  $q = 1$  surface. Though some models [10,11,15] do not require the  $q = 1$  surface,  $q_{\min}$  should be just above unity. On the other hand, in the proposed model, the  $q = 1$  surface is not required because the  $m/n = 1/1$  sideband current directly deforms the plasma, which arrow to excite the non-resonant mode. Our observation and model give the new explanation on the excitation mechanism of the HC.

Though the proposed model successfully explains the characteristics of the coupling, there are some issues to deal with by our model:

- I. Because the only linear phase is considered in section 4, the saturated amplitude of the  $m/n = 1/1$  component of the radial displacement  $(\xi_r)_{1,1}$  is not estimated. As shown in figure 10, when an  $m/n = 2/1$  TM and an  $m/n = 1/1$  HC is observed, the  $\xi_r$  is about  $1 \sim 1.5$  cm in the core region, which seem to be  $(\xi_r)_{1,1}$  in the core region. Note that the relatively high values of  $\xi_r$  around  $\rho \sim 0.6$  near  $q \sim 2$  may be due to the synergy effect of the  $m/n = 2/1$  TM and the  $m/n = 1/1$  HC. The width of the  $m/n = 2/1$  magnetic island is about  $(\delta\rho)_{\text{island}} \sim 0.15$  obtained with CXRS measurement. The validation of the proposed model can be done with the calculation of the saturated  $\xi_r$  profile in the nonlinear MHD simulation.
- II. The  $m/n = 3/1$  structure is not observed in experiments though the structure due to the  $m/n = 3/1$  sideband current can appear with equation (11) in our model. The possible explanation is the difference of the energy required to induce the  $m/n = 1/1$  deformation and the  $m/n = 3/1$  deformation. If the required energy to induce  $m/n = 1/1$  deformation is smaller than the energy to induce  $m/n = 3/1$  deformation, only  $m/n = 1/1$  deformation may be observed. Based on this hypothesis, if the large filament current occurs, the  $m/n = 1/1$  and  $m/n = 3/1$  deformation can be observed simultaneously. It is also required to consider the  $m/n = 4/1$  component induced by the  $m = \pm 2$  component of the metric tensor with the non-circular poloidal cross section, which is ignored in this study.
- III. The effect of the  $q = 1$  surface is not clear in our model. If  $q = 1$  surface exists, the  $m/n = 1/1$  mode localized at the core should occur and perhaps interacts with the  $m/n = 1/1$  HD which is not localized at the core region. This issue is related with the absence of the sawtooth collapse with  $m/n = 2/1$  NTMs introduced in the next paragraph.

In many tokamaks such as DIII-D, it was reported the sawtooth-free hybrid plasma was realized by “flux pumping” with HCs [6,7]. In this study, the sawtooth-free phase is also observed with an  $m/n = 2/1$  NTM as seen in figure 3. In figure 3 (c), the periodic peak of the high coherence around 5 kHz after 10.8 s indicates the  $n = 1$  precursors of the sawtooth collapses. On the precursors, the  $m = 1$  structure is also observed in SX measurement and the mode frequency is consistent with  $f_{\text{tor}}$  in the core region [38]. From these observations, the observed  $n = 1$  precursor seems to be the  $m/n = 1/1$  mode localized at the core region, which is usually observed before the sawtooth collapse [39]. The expanded view on the sawtooth collapses with SX signals is shown in figure 11. The sawtooth collapse is only observed after the  $m/n = 2/1$  NTM is stabilized by ECCD around  $q = 2$  surface ( $\rho = 0.6$ ), though sawtooth collapse may occur at 9.5 s where  $q_{\min} < 1$  as seen in figure 5(d). In this study, however, because the error of the  $q$ -value can be large in the core due to the absence of the measured point as seen in figure 5(d), it cannot be concluded that  $q_{\min} < 1$  with the  $m/n = 2/1$  NTM. The suppression of the sawtooth collapse with the  $m/n = 2/1$  NTM was also observed in DIII-D [40], which is explained by the “flux pumping” induced with the interaction between NTMs and ELMs. The possibility of the suppression of sawtooth collapses in JT-60U with  $m/n = 2/1$  NTMs by dedicated investigations whether  $q_{\min} < 1$  or  $q_{\min} > 1$  will be reported in near future.

## 6. Summary

In this paper, we investigate the excitation condition and the excitation mechanism of the coupling based on the previous study [19]. To investigate the possible excitation mechanism, the  $m/n = 2/1$  NTMs whose mode frequencies are several kHz, are investigated. It is found that the coupling is observed with the mode frequency with several Hz and with 6 kHz. This indicates that the resistive wall and the plasma control system do not induce the coupling. It is also confirmed that  $n = 1$  HCs does not rotate with the plasma in the core region by means of the comparison of the mode frequency  $f_{\text{mode}}$  and the plasma rotation frequency  $f_{\text{tor}}$  in the core region. In addition, it is found that the coupling is observed even when  $q_{\min} > 1$ , indicating that  $n = 1$  HCs are the non-resonant mode. In considering of these observations, we propose the new model where the non-resonant  $m/n = 1/1$  HD is induced directly by the current for the  $m/n = 2/1$  TM, which does not need the corresponding  $q = 1$  surface to allow the excitation of the non-resonant mode. The proposed model on the excitation

mechanism consistency describes the experimental observations of the coupling suggested in the previous study [19] (characteristics (1) ~ (3)) and in this study (the characteristic as the non-resonant mode which is not localized at the core region mentioned in section 3). The main difference from the model proposed by other authors [8,10,11,15] are the requirement of the  $q = 1$  surface. In this study, the sawtooth-free phase with  $m/n = 2/1$  NTMs are also observed, which is similar with the sawtooth-free plasmas induced by HCs in other tokamaks [6,7,18]. The further investigations with the relationship with the  $m/n = 2/1$  NTM and the sawtooth collapse will be reported in near future.

## Acknowledgments

Helpful comments for analysis by Dr T. Suzuki, Dr. N. Aiba and Dr. S. Sumida are greatly appreciated.

## Appendix A: Method to modify the phase in subsection 3.1

If we distinguish the poloidal number in the core, the change of the poloidal angle of the measured points should be around  $\pi$  rad. across  $\rho = 0$ . However, as shown in figure 12 (a), the poloidal angles of ECE measurement in the core region changes  $0.7 \pi$  rad. Therefore, it is required to modify the observed phase considering these poloidal angles to investigate the mode structure. Here, as shown in figure 12 (b), if the measured point before the movement is located as the lower field side from the magnetic axis, the measured point is moved to the point on the midplane in the lower field side keeping the minor radius. In the opposite case, the measured position is moved to the higher field side. This method to modify the phase is valid when the single mode having a certain poloidal number covers the region for the estimation. This method is also affected by the accuracy of the estimation of the MHD equilibrium. The error due to the estimation of the MHD equilibrium is more sensitive near the estimated axis.

## References

- [1] J. G. L. Jahns et al., *Nucl. Fusion* **22** 1049 (1982).
- [2] L. Delgado-Aparicio et al., *Nucl. Fusion* **53** 043019 (2013).
- [3] T. Bando et al., *Phys. Plasmas* **25** 012507 (2018).
- [4] P. Piovesan et al., *Plasma Phys. Control. Fusion* **59** 014027 (2017).
- [5] J.E. Menard et al., *Nucl. Fusion* **45** 539 (2005).
- [6] S. C. Jardin, N. Ferraro, and I. Krebs, *Phys. Rev. Lett* **115** 215001 (2015).
- [7] P. Piovesan et al., *Nucl. Fusion* **57** 076014 (2017).
- [8] J. A. Wesson, *Plasma Phys. Control. Fusion* **37** A337 (1995).
- [9] A. Weller et al., *Phys. Rev. Lett.* **59** 2303 (1987).
- [10] W. A. Cooper et al., *Phys. Rev. Lett.* **105** 035003 (2010).
- [11] W. A. Cooper et al., *Nucl. Fusion* **53** 073021 (2013).
- [12] I. T. Chapman et al., *Nucl. Fusion* **50** 045007 (2010).
- [13] J.A. Breslau et al., *Nucl. Fusion* **51** 063027 (2011).
- [14] A. Wingen et al., *Phys. Plasmas* **26** 022501 (2019).
- [15] I. Krebs et al., *Phys. of Plasmas* **24**, 102511 (2017).
- [16] A. Wingen et al. *Nucl. Fusion* **58** 036004 (2018).
- [17] M. Cianciosa et al. *Nucl. Fusion* **57** 076015 (2017).
- [18] Y. Yuan et al., *Nucl. Fusion* **60** 016003 (2020).
- [19] T. Bando et al., *Plasma Phys. Control. Fusion* **61** 115014 (2019).
- [20] G. Matsunaga et al., *Plasma and Fusion Research* **4** 051 (2009).
- [21] N. Oyama and the JT-60 Team, *Nucl. Fusion* **49** 104007 (2009).
- [22] A. Isayama et al., *Nucl. Fusion* **49** 055006 (2009).
- [23] N. Isei et al., *Rev. Sci. Instrum.* **66** 413 (1995).
- [24] A. Isayama et al., *Rev. Sci. Instrum.* **73** 1165 (2002).
- [25] M. Yoshida et al., *Fusion Eng. Des.* **84** 2206 (2009).
- [26] T. Fujita et al., *Fusion Eng. Des.* **34-35** 289 (1997).
- [27] T. Suzuki et al., *Rev. Sci. Instrum.* **79** 10F533 (2008).
- [28] Azumi M., Kurita G., Matsuura T., Takeda T., Tanaka Y. and Tsunematsu T. 1980 Proc. of the 4th Int. Symp. on Computational Methods in Applied Science and Engineering (Paris,) p 335.
- [29] K. Shinohara et al., *Nucl. Fusion* **47** 997 (2007).
- [30] D. A. Gates and T. C. Hender, *Nucl. Fusion* **36** 273 (1996).



- [31] V. Igochine, *Active Control of Magneto-hydrodynamic Instabilities in Hot Plasmas* (Springer, 2015), Chap. 8.  
 [32] A. Isayama et al., *Plasma Fusion Res.* **5** 037 (2010).  
 [33] M. Honda et al., *Nucl. Fusion* **53** 07305 (2013).  
 [34] N. Aiba et al., *Nucl. Fusion* **57** 022011 (2017).  
 [35] G. Matsunaga et al., *Nucl. Fusion* **50** 084003 (2010).  
 [36] R. Fitzpatrick, *Phys. of Plasmas* **22** 042514 (2015).  
 [37] G. Kim et al., *Plasma Phys. Control. Fusion* **60** 035009 (2018).  
 [38] M. Yoshida et al., *Nucl. Fusion* **52** 023024 (2012).  
 [39] I. T. Chapman et al., *Plasma Phys. Control. Fusion* **53** 013001 (2011).  
 [40] J. D. King et al., *Phys. of Plasmas* **19** 022503 (2012).

$\beta_N$	0.6 ~ 0.8 % m T MA <sup>-1</sup>
$\beta_p$	0.46 ~ 0.68
Total neutron emission rate	1.1x10 <sup>15</sup> ~ 2.5x10 <sup>15</sup> n/s
Plasma current	1.5 MA
Magnitude of magnetic field at magnetic axis	3.7 T
Major radius	3.18 m
Minor radius	0.8 m
Plasma volume	55 ~ 56 m <sup>3</sup>
Radial position of axis	3.23 ~ 3.25 m
Vertical position of axis	0.10 ~ 0.11 m
Plasma triangularity	0.18 ~ 0.20
Plasma elongation	1.4 ~ 1.5
q <sub>95</sub> (the safety factor on 95% of flux surface)	4.05 ~ 4.09
Plasma-wall separation in low field side	0.58 ~ 0.60 m

Table 1: The plasma parameters of 39 discharges where  $m/n = 2/1$  NTMs with  $n = 1$  HCs, whose mode frequencies are several kHz, are observed. The analyzed discharges are made after the installation of ferrite steel tiles on the vacuum vessel to reduce the toroidal magnetic field ripple [29].

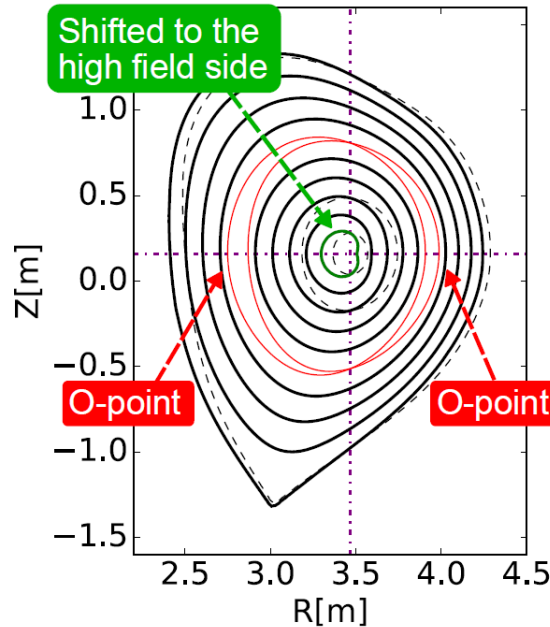


Figure. 1. Schematic view of the poloidal cross sections showing the phases of the  $m/n = 2/1$  TM and the  $m = 1$  HC based on the view of the coupling described in the previous paper [19]. The core is shifted to the high-field side when the O-points of the  $m/n = 2/1$  magnetic island line up in the midplane. To keep this configuration, the  $m/n = 2/1$  TM and the  $n = 1$  HC have to rotate satisfying  $f_{m/n=1/1(HC)} = 2f_{m/n=2/1(TM)}$ . The red curves represent the  $m = 2$  magnetic island. The black and green curves show the flux surfaces with  $m = 1$  deformation. The black dashed lines show the flux surfaces at  $\rho \sim 0.1, 0.3, \text{ and } 1.0$  without  $m = 1$  deformation. The cross points of the purple dashed lines show the magnetic axis without  $m = 1$  deformation. The deformed flux surfaces are obtained by adding artificial  $m/n = 1/1$  deformation and artificial  $m/n = 2/1$  magnetic islands to the axisymmetric equilibrium.

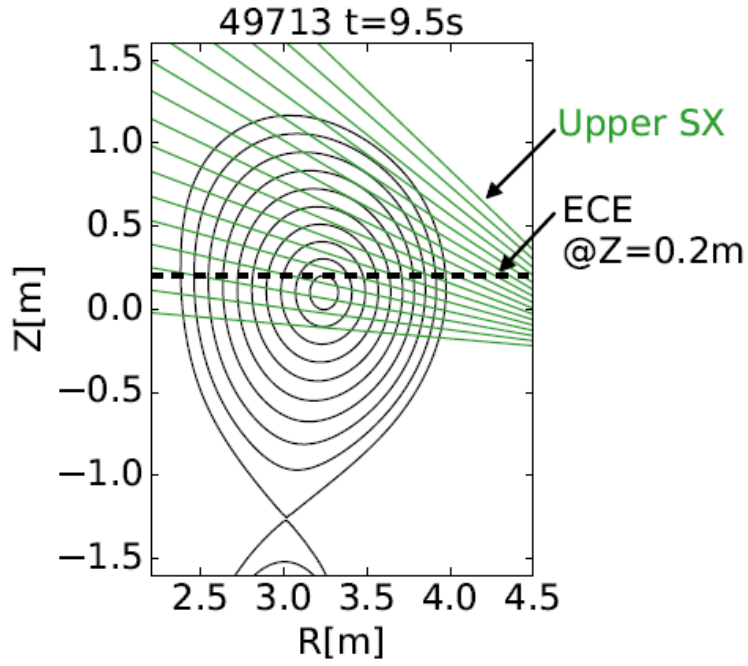


Figure. 2. The sight lines of SX measurement and the measured plane by ECE measurement. The difference in the toroidal angles between the locations of SX measurement and ECE measurement are about 160 degrees. The MHD equilibrium is obtained at 9.5s of 49713.

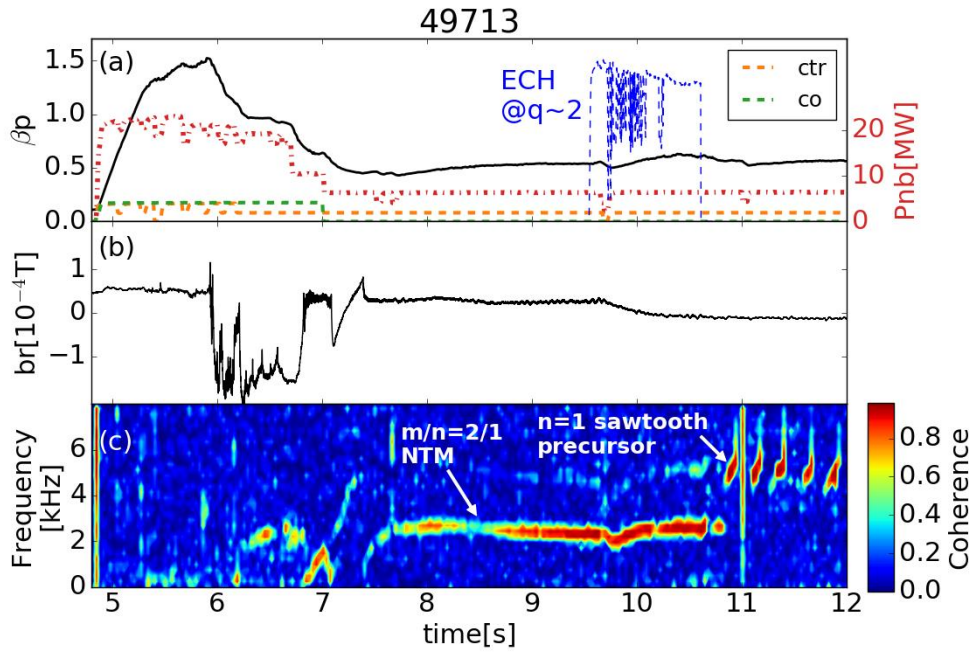


Figure. 3. Time evolution of the signals from an experiment of the stabilization of  $m/n = 2/1$  NTMs by ECCD in JT-60U: (a) the poloidal beta and the total injection power of NBIs (dotted-dashed red line), the injection power of NBIs with ctr-direction and co-direction (orange and green dashed lines), and the pulse pattern of the ECH around  $q = 2$  surface (blue dashed line), (b) the radial component of magnetic fluctuations,  $b_r$ , obtained with saddle loops and (c) the spectrum of coherence of SX signals from a slight line viewing the core and the magnetic fluctuation. An  $m/n = 2/1$  NTM is excited around 5.92 s in the current flat-top phase.

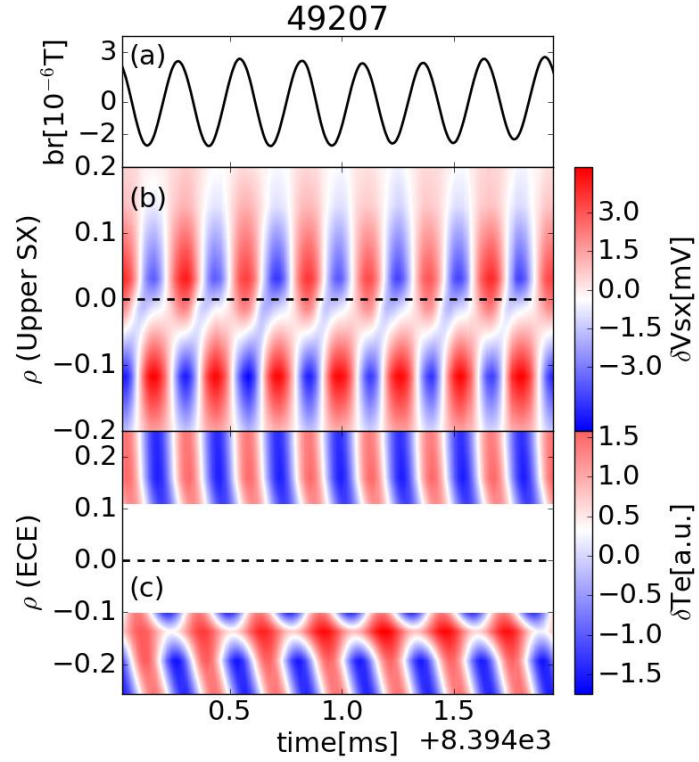


Figure 4. The time evolution of (a) the magnetic fluctuation, (b) the radial profile of the fluctuation component of SX signals from Upper SX, and (c) the radial profile of the fluctuation component of the electron temperature measured by ECE measurement when an  $m/n = 2/1$  NTM is observed in 49207. The horizontal black dashed lines in (b) and (c) indicate  $\rho = 0$ .

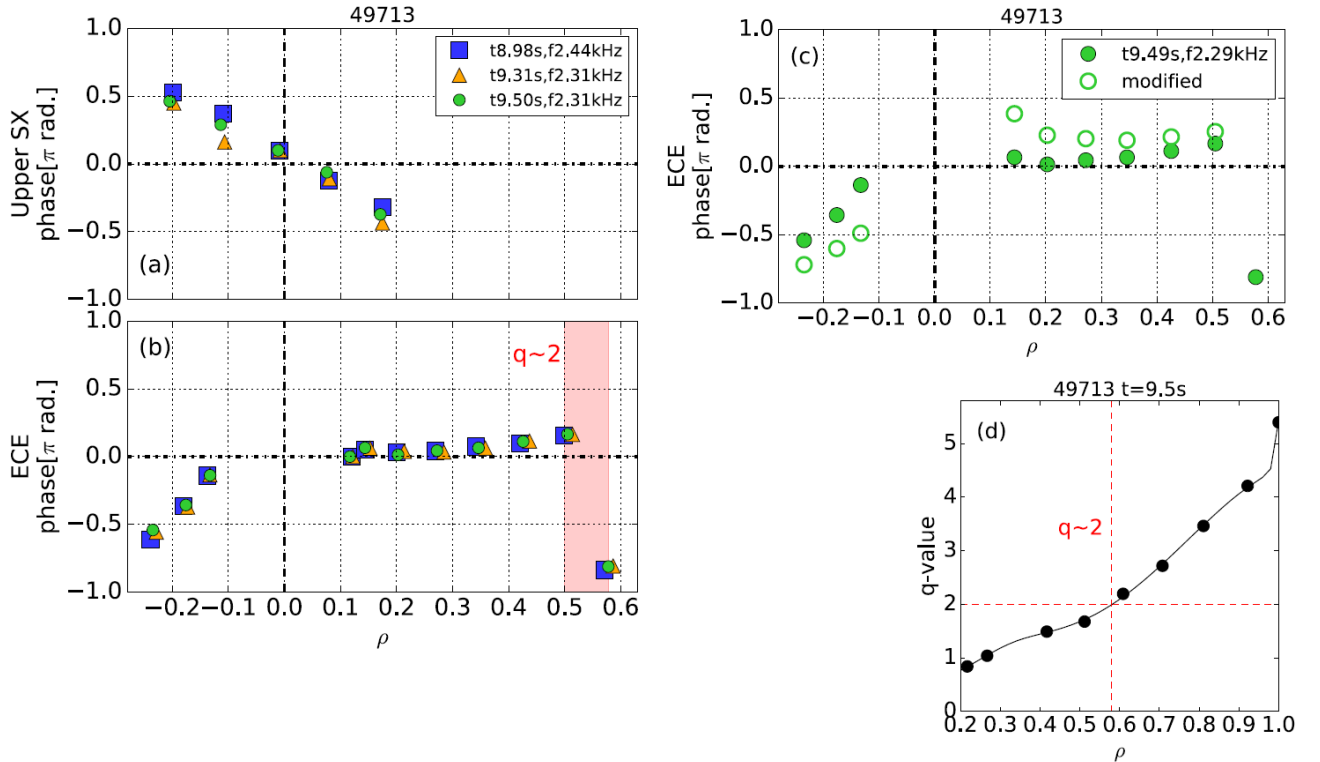


Figure 5. The radial profile of the phase obtained with cross spectrum of Fourier transform at 9 s, 9.3 s, and 9.5 s from (a) SX measurement and (b) ECE measurement. (c) The radial profile of the phase and the modified phase at 9.5 s. (d) The  $q$ -profile at 9.5 s obtained with MSE measurement and the MEUDAS code. In (a), (b), and (c), the coherence is calculated between the channel viewing near the axis and other channel. In (c), the data with the poloidal angle  $\sim 0.5 \pi$  rad. is not shown because the error of the modification near the axis can be large as explained in Appendix A. In (d), the black circles are the estimated safety factor of MSE channels. Because the measure points do not exist in the core region  $\rho < 0.215$ , the  $q$ -profile is not shown in the core region.

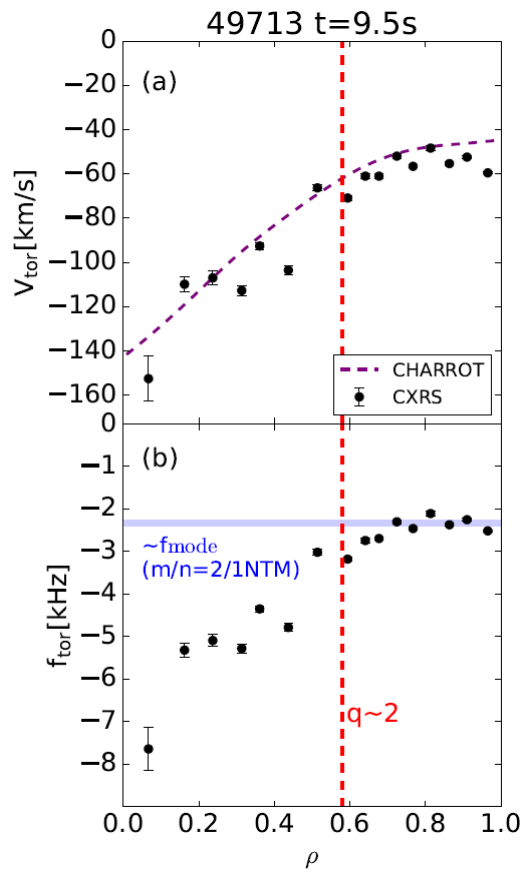


Figure. 6. The radial profile of the toroidal velocity ( $V_{\text{tor}}$ ) and the toroidal rotation frequency ( $f_{\text{tor}}=V_{\text{tor}}/2\pi R_m$ ) measured by CXRS measurement at 9.5 s. Here,  $R_m$  is the major radius where  $V_{\text{tor}}$  is measured. In (a), the purple dashed line is the toroidal velocity of background deuterium plasma estimated by the CHARROT code [33,34]. In (b),  $f_{\text{mode}}$  is the observed mode frequency of the  $m/n = 2/1$  NTM.

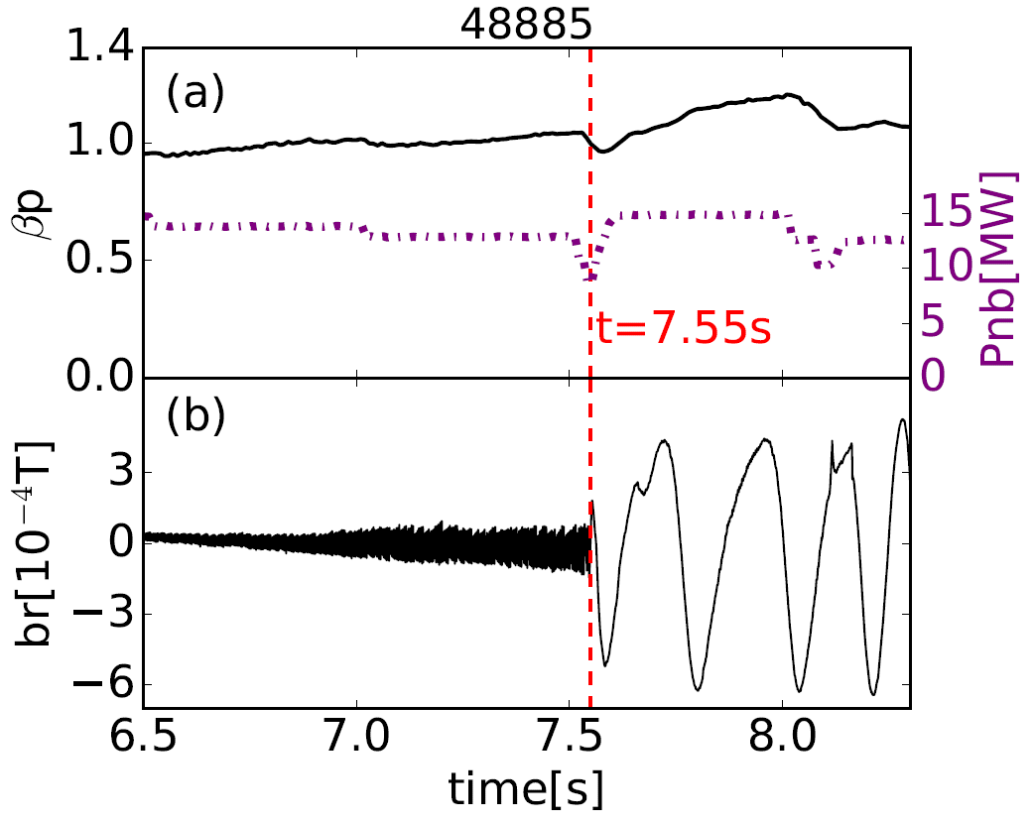


Figure 7. Time evolution of the signals from an experiment when an  $m/n = 2/1$  TM is observed in JT-60U: (a) the poloidal beta and the total injection power of NBIs (dotted-dashed purple line) and (b) the magnetic fluctuation.

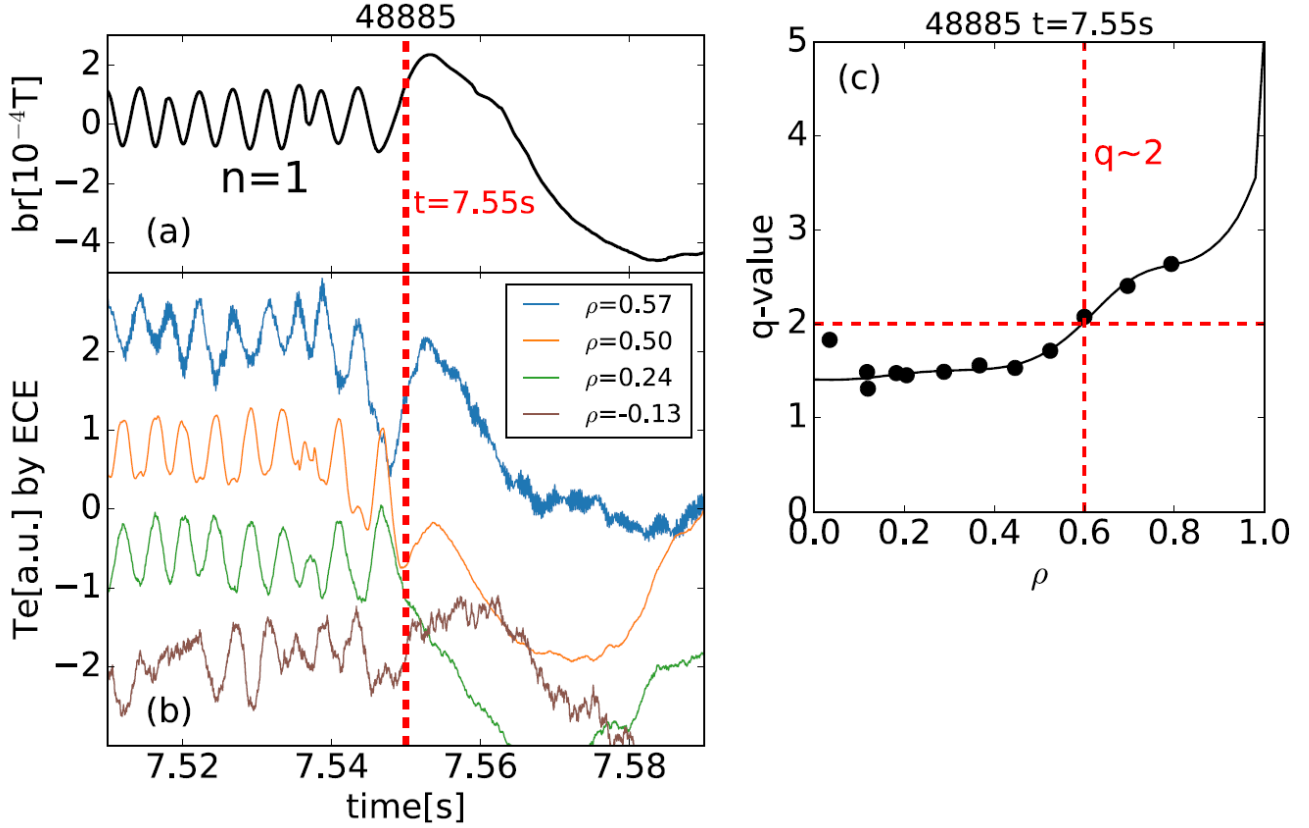


Figure 8. The time evolution of (a) the magnetic fluctuation and (b) the electron temperature at  $\rho = -0.13, 0.24, 0.50$  and  $0.57$ . (c) The  $q$ -profile at  $7.55$  s estimated with MSE measurement and the MEUDAS code. In (c), the black circles are the estimated safety factor of MSE channels.

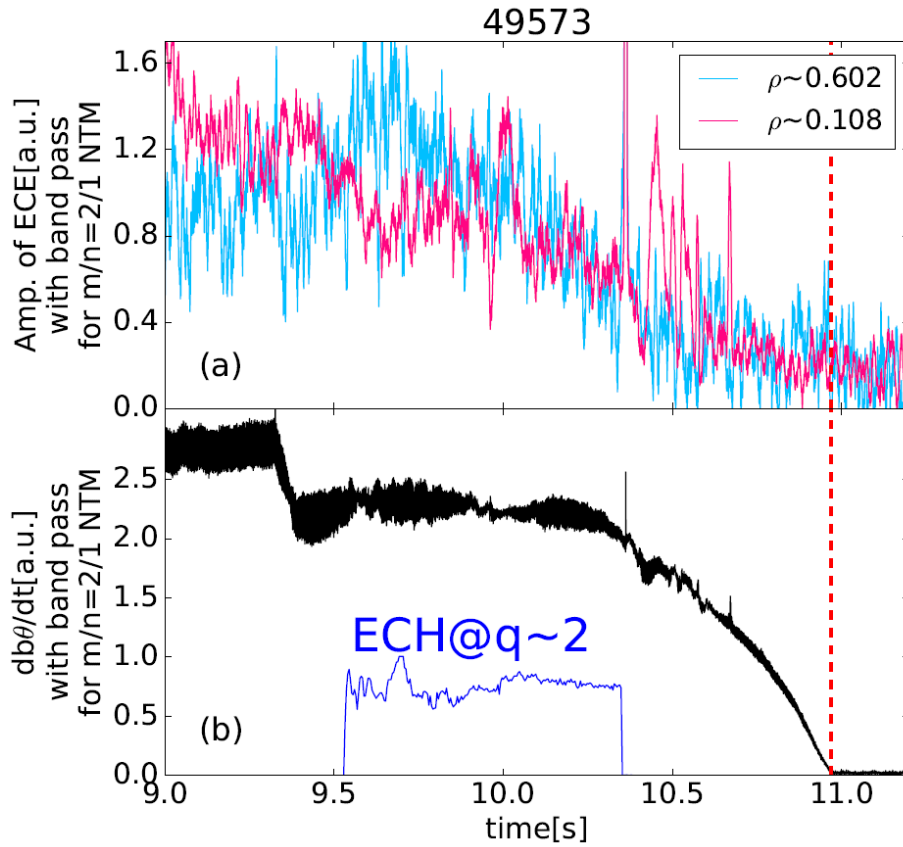


Figure 9. The time evolution of (a) amplitudes of signals from ECE measurement and (b) the magnetic fluctuation with the band pass filter to obtain the component due to  $m/n = 2/1$  NTM. In (a), the signals measured at  $\rho = 0.108$  and  $0.602$  are shown. In (b), the blue line indicates the pulse pattern of ECH (ECCD) around  $q = 2$  surface to stabilize the  $m/n = 2/1$  NTM. The  $m/n = 2/1$  NTM is stabilized around 11 s according to the magnetic fluctuation.

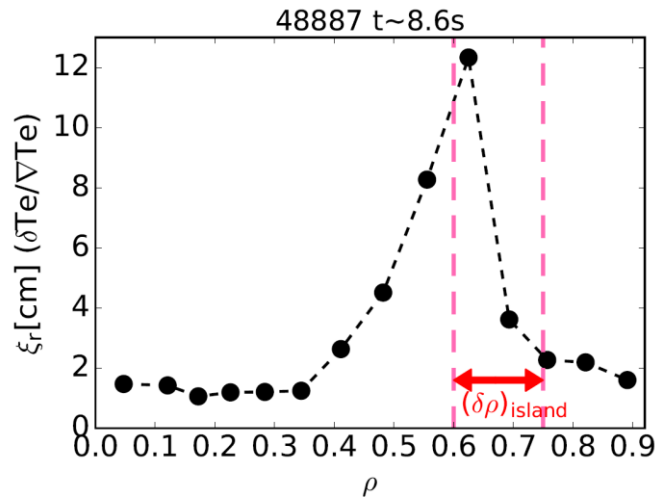


Figure 10. The profile of the radial displacement  $\xi_r$  estimated with ECE measurement around 8.6 s in 48887 when an  $m/n = 2/1$  TM and an  $m/n = 1/1$  HC is observed.  $\xi_r$  is estimated as  $\delta T_e/\nabla T_e$ . Here, the mode frequency of the  $m/n = 2/1$  NTM is about 4 Hz. The MHD equilibrium is calculated at 8.66 s. The region where the flattening of the ion temperature profile obtained with CXRS measurement is shown by the red arrow.

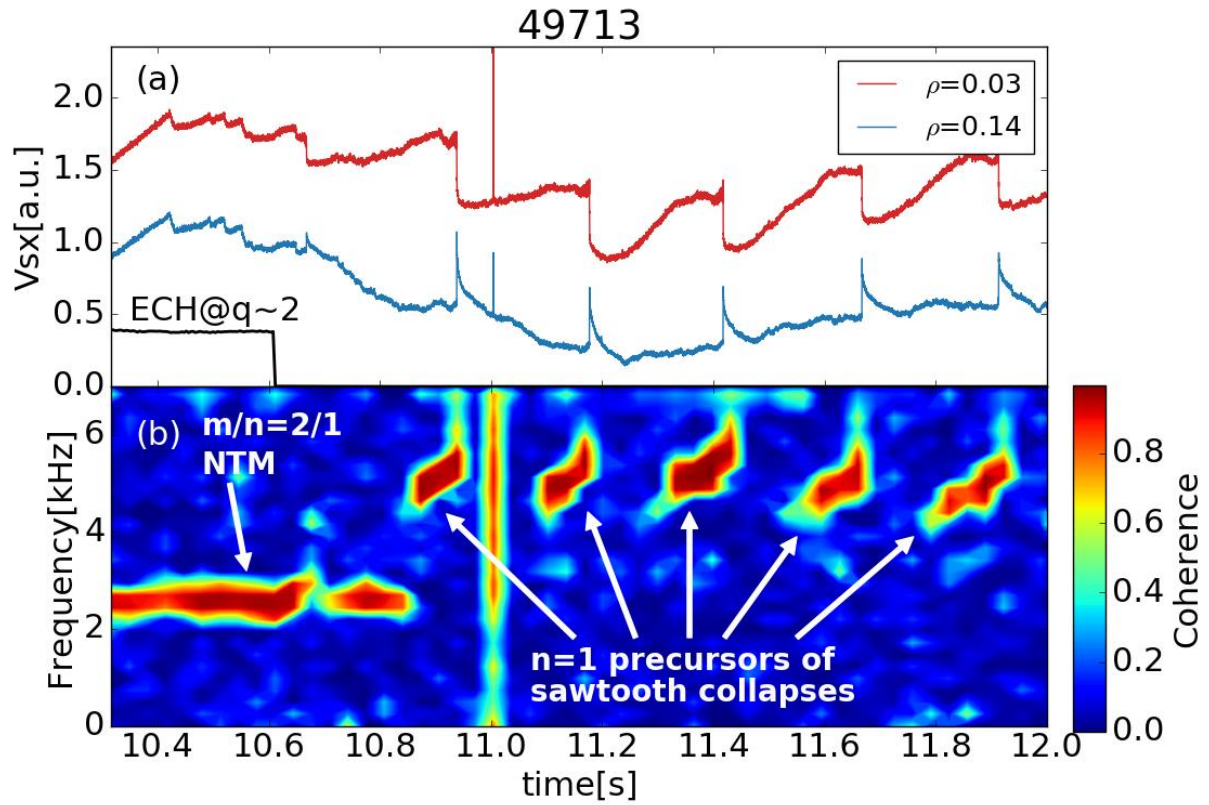


Figure. 11. The time evolution of (a) amplitudes of signals from SX measurement and (b) the spectrum of coherence of SX signals from a slight line viewing the core and the magnetic fluctuation. In (a), the signals viewing at  $\rho = 0.03$  and  $0.14$  are shown. The black line indicates the pulse pattern of ECH (ECCD) around  $q = 2$  surface to stabilize the  $m/n = 2/1$  NTM. The sawtooth collapses are observed repeatedly with  $n = 1$  precursors after the stabilization of the  $m/n = 2/1$  NTM by ECCD.



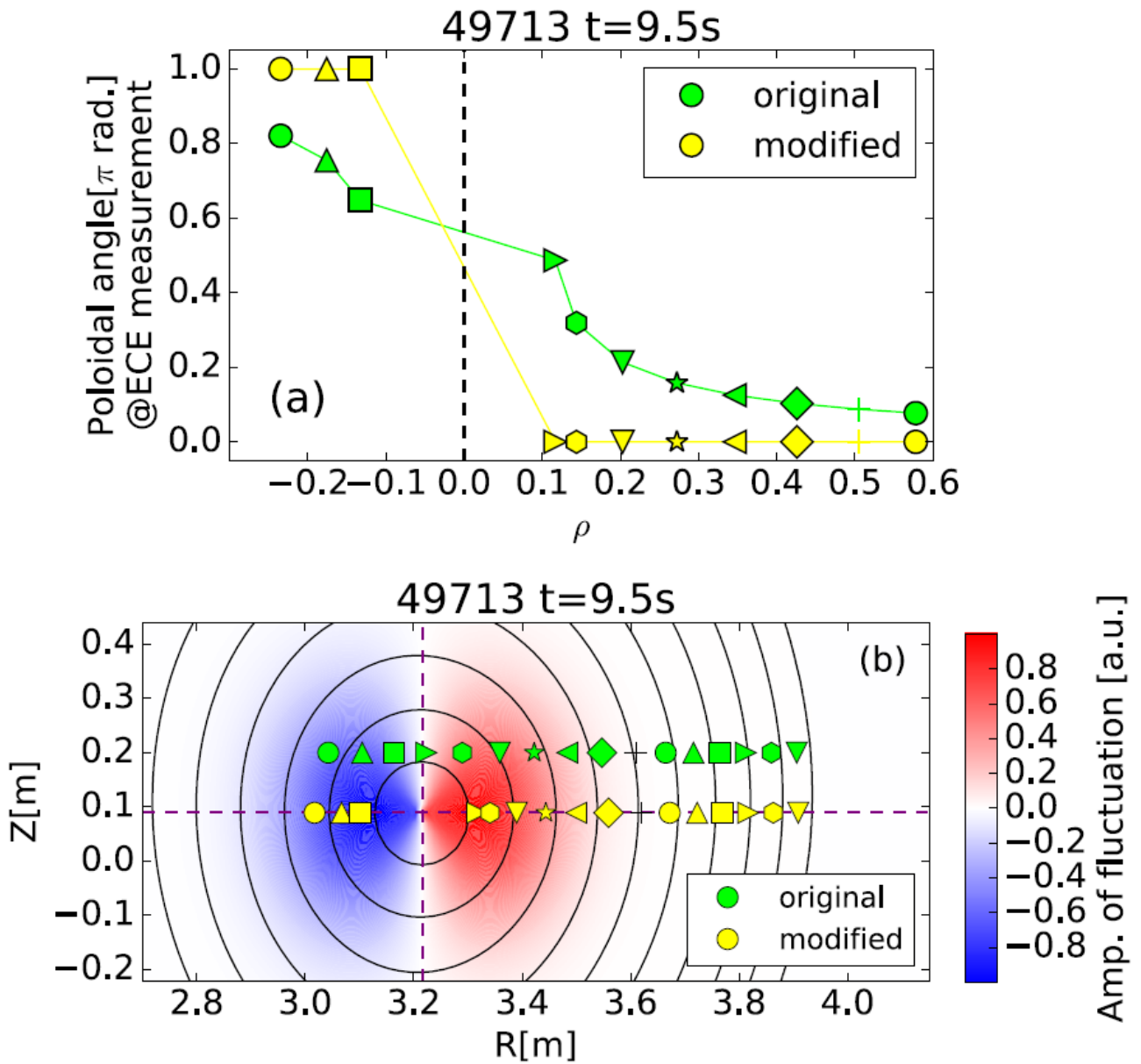


Figure. 12. (a) The radial profile of the poloidal angle measured by ECE measurement. (b) The flux surfaces in a poloidal cross section and the measured positions of ECE measurement. In (b), the contour map shows the amplitude of the fluctuation of an  $m = 1$  mode in the core region. In figure (a) and (b), the green and yellow markers mean the original measured poloidal angles (points) by ECE measurement and the modified measured poloidal angles (points) with the method explained in Appendix A, respectively.